Photonic BiCMOS Technology with 80 GHz Ge Photo Detectors and 100 GHz Ge Electro-Absorption Modulators

D. Steckler[1], S. Lischke[1], A. Peczek[1], A. Kroh[1] and L. Zimmermann[1,2]
[1]IHP - Leibniz Institut für innovative Mikroelektronik, 15236 Frankfurt (Oder), email: steckler@ihp-microelectronics.com
[2]Technische Universität Berlin, FG Silizium-Photonik, 10587 Berlin

***Abstract*—**We demonstrate a Photonic BiCMOS technology featuring waveguide-coupled germanium electro-absorption modulators and photo detectors with respective 3-dB bandwidths of 100 GHz and 80 GHz, monolithically integrated with high-performance SiGe-heterojunction bipolar transistors and 0.25 µm CMOS. The electro-absorption modulators feature insertion losses of 7.5 dB and dynamic extinction ratios of 3.6 dB at 2 V_{pp} and λ = 1600 nm. We demonstrate that there is no degradation of the baseline technology 'SG25H5EPIC' in terms of electronic device yield or performance.

I. Introduction and Motivation

Over the past decade, silicon photonics has become a major technology in fiber optical communication. The absence of an efficient modulation mechanism on silicon is a serious bottleneck to integration, though. Mach-Zehnder modulators (MZMs) based on carrier dispersion tend to exhibit comparatively large footprints prohibitive for dense transmitter arrays. At present, resonant ring modulators (RRMs) are studied intensely as a more compact alternative. However, RRMs suffer from typical issues of resonant devices such as significant temperature sensitivity, process variations as well as wavelength and power dependence. In addition, RRMs show limitations regarding OE bandwidth similar to plasma dispersion MZMs. Most devices have been confined to a bandwidth below 50 GHz, and exceptional 67 GHz, recently [1, 2, 3]. Targeting 100-200 GBaud symbol rates, this necessitates extensive transmitter side equalization and signal processing detrimental to power efficiency. Silicon technology compatible modulator devices with opto-electrical (OE) bandwidth approaching 100 GHz are therefore highly desirable. One promising candidate for faster and more energy-efficient transmitters with small footprint are Electro-Absorption modulators (EAMs), exploiting the Franz-Keldysh-Effect (FKE). Recently, Ge EAMs with 3-dB bandwidth > 110 GHz operating at L-Band wavelengths were demonstrated [4]. CMOS inverter based drivers have been shown to efficiently drive RRMs. In contrast to RRMs, EAMs generate considerable photocurrent due to absorption. SiGe BiCMOS drivers excel in handling large currents at high frequency. We therefore invested in monolithic frontend-of-line co-integration of high-performance BiCMOS electronics and silicon photonics including high-bandwidth EAMs and photo diodes. Both, the RF performance and energy-efficiency benefit from the absence of large parasitic capacitances and inductances that typically occur due to required bond pad sizes in hybrid integration approaches. Our technology will significantly benefit dense optical I/O applications such as multi-chiplet GPU interconnects [5].

In this work we present, high-speed Ge EAM that are monolithically integrated in IHP's photonic BiCMOS technology:

(1) The Ge EAMs feature state-of-the-art 3-dB EO bandwidths of 100 GHz together with insertion losses and dynamic extinction ratios of 7.5 dB and 3.6 dB, respectively.
(2) Co-integration with Ge photo detectors providing OE bandwidths of 80 GHz and moderate internal L-band responsivities of ~ 0.5 AW^{-1}.
(3) To ensure sufficiently low EAM insertion loss we re-utilized a Si dry etch for SOI rib-waveguides within the germanium epitaxy windows, without any additional mask effort.
(4) We demonstrate that this process provides high device yields, a prerequisite for the fabrication of transceiver circuitry.

II. Device Concept and Fabrication

IHP's photonic BiCMOS process combines, by means of monolithic frontend-of-line integration, state-of-the-art silicon photonics functionality with high-performance SiGe-heterojunction bipolar transistors (HBT) [6]. This is enabled by providing bulk-Si regions, strongly required for high-performance SiGe-HBT, next to Silicon-on-Insulator (SOI) regions, which are prerequisite for low-loss optical waveguides. Electronic and photonic devices, share a common 5 layers AlCu back-end-of-line. Details on the baseline process and the so-called 'local SOI' formation are provided in [6] and [7], respectively. Photo detection is enabled by germanium p-i-n diodes that are manufactured by selective epitaxial growth of Ge on a locally exposed Si waveguide (WG) region. Encapsulation of the Ge with a differentially grown Si layer allows for application of $CoSi_2$ layer formation in order to achieve low-ohmic contact scheme. Details on the Ge PD fabrication can be found in [9]. In this work we demonstrate that the Ge PD, by few adjustments, can simultaneously be utilized as EAM as well.

While optical coupling from the Si WG into the absorbing Ge works sufficiently well in the case of the photo detector, the requirements are much more stringent for the EAMs. In order to improve mode-matching between Si WG and EAM we locally reduce the Si thickness below the Ge. This is achieved without additional process or mask effort, by utilizing the Si dry etch originally applied to form rib WGs for Si-Mach-Zehnder-modulator phase-shifters. Through this adaptation, the Si thickness is reduced from 220 nm to 100 nm before the Ge epitaxy window is being opened.

Although PD and EAM were realized simultaneously from the same basic device structure, there is some potential for separate optimization as widths and length can be adjusted independently. In this first demonstration, we refrained from additional mask effort which e.g. would allow for separate tuning of doping profiles for both devices or provide flexibility in the adjustment of the Si thickness below the Ge. By decoupling the Si dry etch from the rib-WG formation we see potential to further reduce the insertion loss. Moreover, we omitted Si incorporation into the Ge, which is a common method to enable EAM functionality in the C-band [10]. Therefore, in this work we focus on the device functionalities and performances at L-Band wavelengths, for both, Ge PD and EAM.

III. Measurement Results and discussion

Device cross sections of the Ge PD and EAM are provided in Fig. 1, showing the different Si thicknesses below the Ge as well. As seen in Fig. 2, EAM dark currents are slightly increased compared to those of the PDs, which might be due to the Si dry etch. However, at higher reverse bias, the dark currents are at a similar level ($\leq$ 100 nA at -4 V).

Frequency response behavior of Ge PD is provided in Fig. 3. At -2 V, the Ge PDs exhibit 3-dB OE bandwidth of 80 GHz, estimated at 1600 nm wavelength. Photocurrents plotted versus optical power for the estimation of internal (at the photo diode) and external (at the fiber tip) responsivities are provided in Fig. 4. At 1600 nm, responsivities yield to > 0.33 and > 0.45 AW^{-1}, at -2 V and -4 V, respectively. We attribute the responsivity increase at higher reverse bias to the Franz-Keldysh-Effect. The nonlinear increase of the photocurrent with respects to the optical power, is most likely caused by a shrinkage of the bandgap due to thermal effects. For an input power of 4.8 dBm (at fiber tip) responsivity of 0.63 AW^{-1} is observed. Bias dependent photo- and dark currents are shown in Fig. 5.

The EAMs exhibit bandwidths of ~85 GHz and 100 GHz at bias of -1 and -3 V, respectively (Fig. 6). The bias dependency can be attributed to decreasing capacitance at higher reverse bias (Fig. 7).

The Ge EAMs insertion loss and static extinction ratio for wavelengths from 1550 nm to 1630 nm are shown in Fig. 8. At 1600 nm, the device shows insertion loss of 7.5 dB together with static extinction ratio of 4.5 dB (-3 V). We suspect that the insertion loss is dominated by the coupling losses between Si WG and Ge, as well as by free-carrier-absorption in the highly doped Ge and Si regions. As mentioned earlier, we see certain optimization potential for the EAM through additional mask effort.

In Fig. 9 we provide eye diagrams for data rates of 56 Gb/s up to 80 Gb/s in order to emphasize the RF capabilities of the Ge EAM. We attribute the obvious degradation of the eye-diagrams at higher data rates to limitations of our measurement setup. In fact, the electrical amplifier and the photo diode right before the 60 GHz sampling scope have 3-dB bandwidths of only 70 GHz. The electrical eyes (captured after the electrical amplifier) already show a clear deterioration at high data rates (Fig. 10). Given the frequency response behavior we assume that the EAM should certainly allow for efficient modulation at > 100 GBaud.

As part of routine process control measurements, we investigate not only on integrity and performance of single devices but also their yield. To evaluate the SiGe HBT yield of the photonic BiCMOS process, we chose the ideality factor of the collector current, n_{IC}, from an HBT-array (4096 devices in parallel) as yield criteria (Fig. 11). CMOS yield is confirmed by monitoring bit error rates of an SRAM cell, provided for one representative wafer in Fig. 12. High-frequency behavior of SiGe HBT is demonstrated in Figs. 13 and 14, respectively, showing f_T and f_{max} of ~240 GHz and ~280 GHz. Ring-oscillator gate delays of τ_{Gate} = 3.45 ps are provided in Fig. 15. These results not only confirm unaffected baseline device integrity but also emphasize suitability of this technology for complex transceiver applications.

In Table 1 we compare various Si photonics platforms by means of their modulator performance to benchmark our results.

IV. Conclusion

In this paper we demonstrated, for the first time, a photonic BiCMOS technology comprising both, high-speed Ge PDs and EAMs, with 3-dB bandwidths of 80 and 100 GHz, respectively. The Ge EAM features insertion loss of 7.5 dB and dynamic extinction ratio of 3.6 dB at 2 V_{pp} and λ = 1600 nm. Ge PD responsivity at λ = 1600 nm is around 0.5 AW^{-1} (-4 V), while dark currents remain at moderate levels (< 500 nA at -4 V). To enable efficient coupling between the Si waveguide and Ge, a Si dry etch was re-utilized, without any additional mask. The co-integration of 100 GHz EAMs and state-of-the-art SiGe HBTs will enable the design of energy-efficient, small-footprint transmitters for systems operating at more than 100 GBaud.

References

[1] A. Mohammadi et al., Optical Fiber Communications Conf. and Exhibition (2022), Th3C.1, San Diego, CA, USA, pp. 1-3.

[2] M. Li et al., Photon. Res. 6, 109-116 (2018)

[3] X. Wu et al., 2023 IEEE Silicon Photonics Conference (2023), pp. 1-2, doi: 10.1109/SiPhotonics55903.2023.10141969

[4] X. Hu et al., Optical Fiber Communications Conf. and Exhibition (2023), Th4A.3, pp. 1-3, doi: 10.1364/OFC.2023.Th4A.3.

[5] S. Zhang *et al*., in *IEEE Micro*, vol. 43, no. 2, pp. 86-95, 1 (2023)

[6] S. Lischke et al., Proc. SPIE 11088 (2019), doi: 10.1117/12.2530143

[7] D. Knoll et al., ECS Trans. 50 297 (2013)

[9] S. Lischke et al., Opt. Express 23, 27213-27220 (2015)

[10] J. Liu, Opt. Express 15, 623-628 (2007)

[11] S. A. Srinivasan et al., Journal of Lightwave Technology, vol. 34, no. 2, pp. 419-424 (2016)

[12] https://www.imec-int.com/en/integrated-photonics (accessed July 12, 2023)

[13] S. Y. Siew et al., Journal of Lightwave Technology, vol. 39, no. 13, pp. 4374-4389, July (2021)

[14] A. Rahim et al., Adv. Photon. 3(2) 024003 (2021), https://doi.org/10.1117/1.AP.3.2.024003

[15] D. A. B. Miller, Opt. Express 20, A293-A308 (2012)

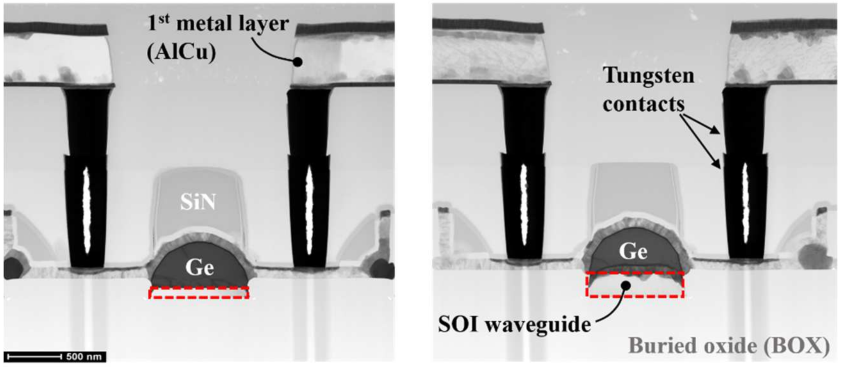

Fig. 1: TEM images of EAM (left) and PD (right). Cross sections cut perpendicular to the light-incidence direction. Images show fabrication up to the first metal layer. The Si thickness below the Ge body has been reduced to 100 nm for the EAM, while in case of the PD the Si thickness remains 220 nm (indicated by dashed red boxes).

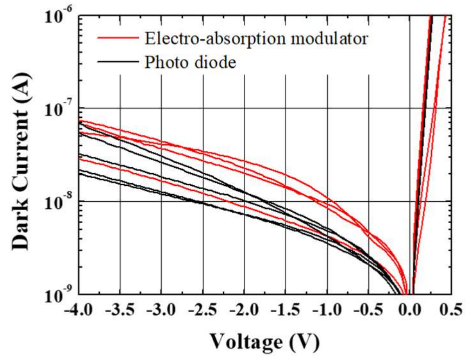

Fig. 2: Room temperature dark currents of PDs and EAMs from -4 V to 0.5 V. (5 representative chips each).

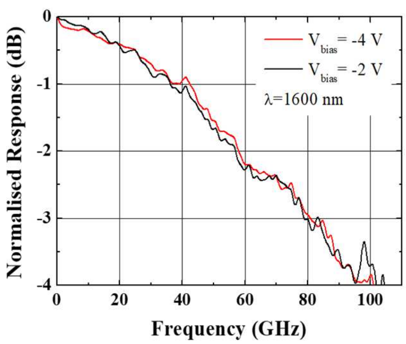

Fig. 3: Normalized S_{21} frequency response of photodiode at wavelength of 1600 nm at -2 V and -4 V for optical input power of P_{in} = 0 dBm at fiber tip, estimated on Keysight 110 GHz LCA.

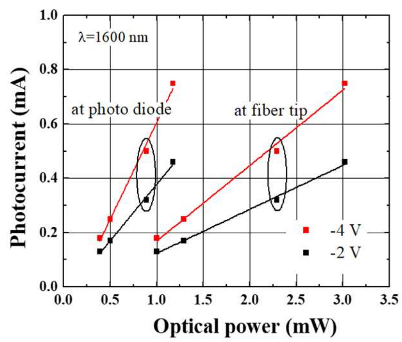

Fig.4 Photocurrents vs optical power to estimate the internal (at the photodiode) and the external (at the fiber tips) responsivity for bias of -2 V and -4 V. The grating coupler losses are about 4 dB at 1600 nm.

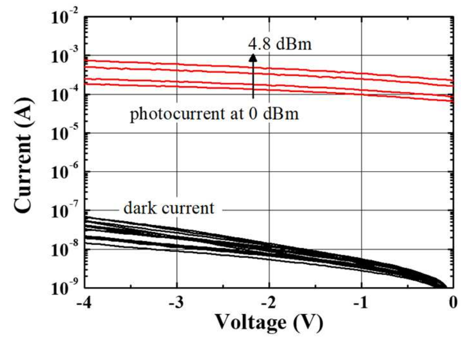

Fig.5 Dark currents measured from -4 V to 0 V (measured on 15 Chips) and photocurrents (for one representative chip) for various input powers at λ = 1600 nm.

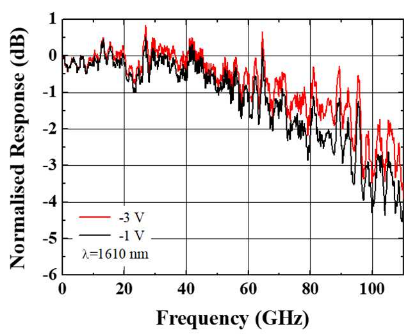

Fig. 6: Normalized frequency response of EAM at wavelength of 1610 nm at bias of -1 V and -3 V for an optical input power of P_{in} = 6 dBm at fiber tip, estimated on Keysight 110 GHz LCA.

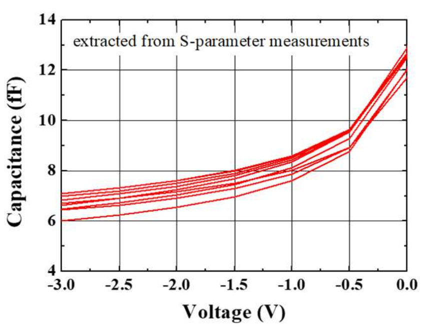

Fig. 7: Capacitance vs. voltage characteristics extracted from S-parameter measurements from Ge PD (measured on 8 wafer sites).

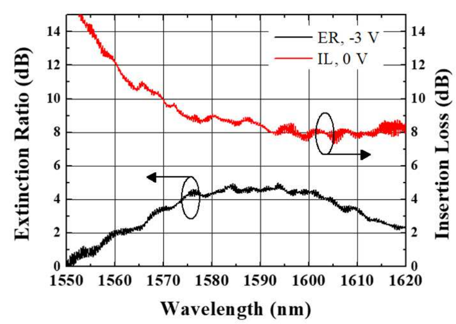

Fig. 8: Static extinction ratio at -3 V and insertion loss of EAM for wavelengths from 1550 nm to 1620 nm (optical input power of 6 dBm).

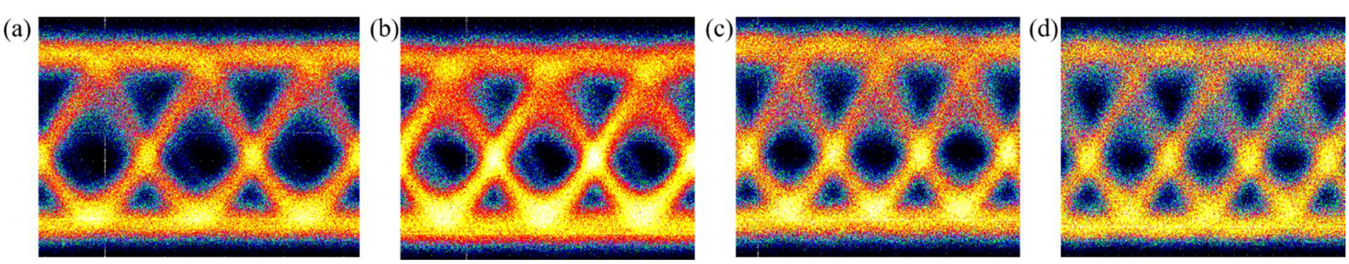

Fig. 9: Eye diagrams of EAM at data rates of 56 Gb/s (a), 64 Gb/s (b), 72 Gb/s (c) and 80 Gb/s (d). The dynamic extinction ratios are 3.6 dB (56 Gb/s), 3.15 dB (64 Gb/s), 3.05 dB (72 Gb/s) and 2.9 dB (80 Gb/s) at bias V_{bias} = -1.5 V and RF signal of 2 V_{pp}. CW light (λ = 1600 nm) was coupled into the EAM at optical power of 6 dBm (at fiber tip). The modulated optical signal was amplified by an EDFA, converted to the electrical domain by a PD and displayed on a sampling scope.

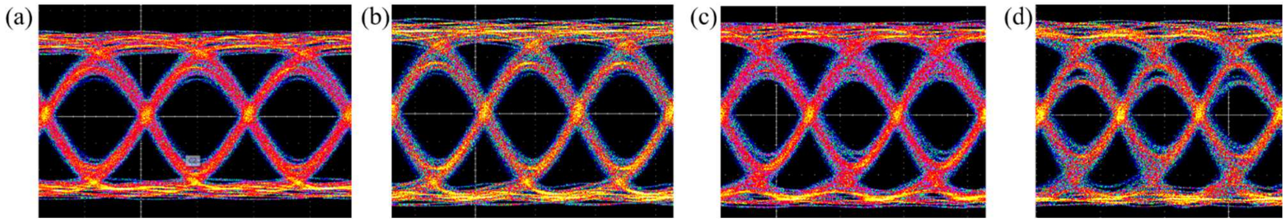

Fig. 10: Electrical signal used to drive the EAM at data rates from 56 Gb/s (a), 64 Gb/s (b), 72 Gb/s (c) and 80 Gb/s (d). A pseudo-random-bit-sequence with a word length of 2^7-1 was generated by a commercial arbitrary waveform generator. The output signal with 0.5 mV_{pp} was then amplified to 2 V_{pp} and used to drive the EAM through a bias-tee and radiofrequency probes.

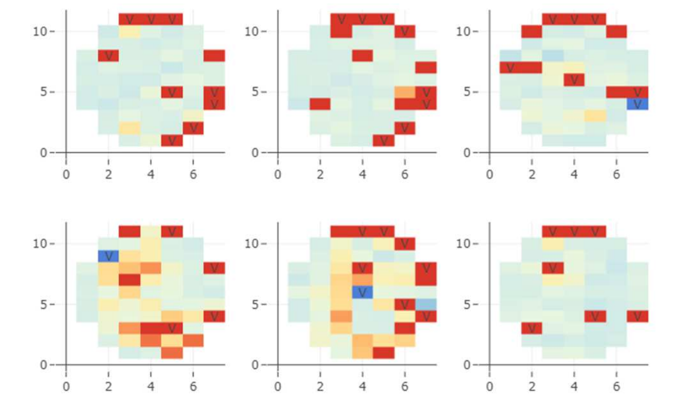

Fig. 11: Collector current ideality factor, n_{IC}, from an array consisting of 4096 SiGe HBTs (connected in parallel), for the sake of presentation shown for six wafers from the same lot. High yield > 80 % is achieved with the criteria of $n_{IC} < 1.05$ at $V_{BE} = 0.5$ V (red chips are out of spec).

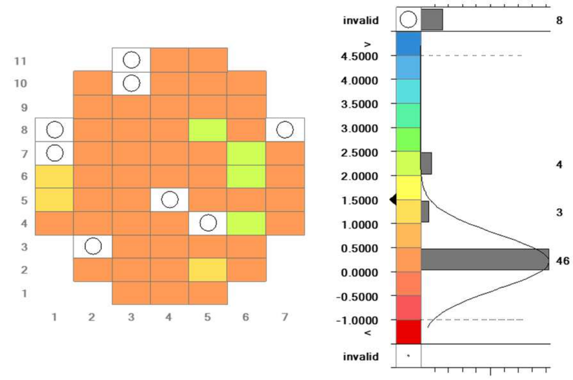

Fig. 12: Wafermap of bit error rate for '0.25 Mbit SRAM' cell (contains ~1.5M CMOS gates). With criteria of bit error rate BER=0, yield is ~75 %. Seven chips have very few BER ≤ 2 (in yellow and green).

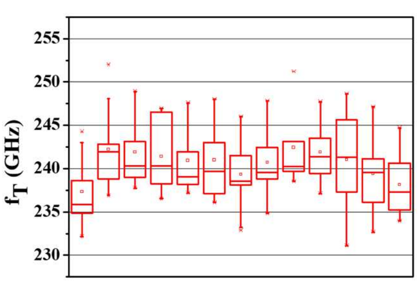

Fig. 13: Box-plots of unity gain frequency, f_T, measured on 13 wafers from one lot, 9 chips measured on each wafer.

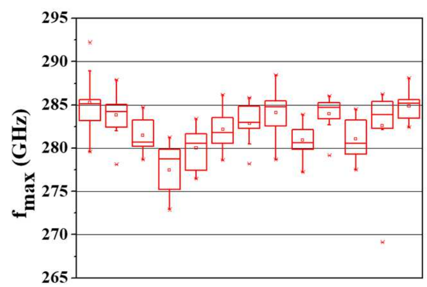

Fig. 14: Box-plots of maximum oscillation frequency, f_{max}, measured on 13 wafers from one lot, 9 chips measured on each wafer.

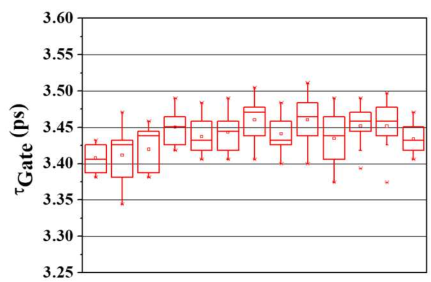

Fig. 15: Box-plots of ring-oscillator gate delay, τ_{Gate}, measured on 13 wafers from one lot, 9 chips measured on each wafer.

	imec [11]	Intel [3]	imec [12]	CEA-Leti [13]	AMF [13]	This work
Platform	PIC	PIC	PIC	PIC	PIC	EPIC
Modulator type	EAM	RRM	RRM	MZM	MZM	EAM
Resonant device	No	Yes	Yes	No	No	No
Dynamic Extinction Ratio (dB)	3.3 (2 V_{pp})	3.4 (1.8 V_{pp})	–	–	3.9 (3 V_{pp})	3.6 (2 V_{pp})
Insertion Loss (dB)	4.9	6	–	2.4	4	7.5
Device Length or Radius (µm)	40	4	5	3000	4000	20
Calculated dynamic power consumption (fJ/bit)	13.8	20.25	25	⁑	⁑	7.5
EO bandwidth (GHz)	> 50*	62	45	40	> 40	100
Operational window	C-, L-Band	O-, C-, L-band	O-, C-, L-band	O-, C-, L-band	O-, C-, L-band	L-Band

Table 1: Overview of state-of-the-art Si-based modulators available in recent silicon photonics platforms. We compare Mach-Zehnder Modulators (MZM) to resonant ring modulators (RRM) and Electro-Absorption modulators (EAM) as more compact device alternatives. For fair benchmarking we compare dynamic ER at V_{pp} = ~2 V and 56 Gb/s, if applicable (in Ref. [3], dynamic ER was estimated at 128 Gb/s).
* Measurement limited to 50 GHz;
⁑ No information found in reference. MZMs typically have a dynamic power consumption of around 200 fJ/bit [14].
The dynamic power consumption has been calculated with $\Delta E_{bit} = ¼(CV_{pp}^2)$ [15]